ARGESIM Report no. 10

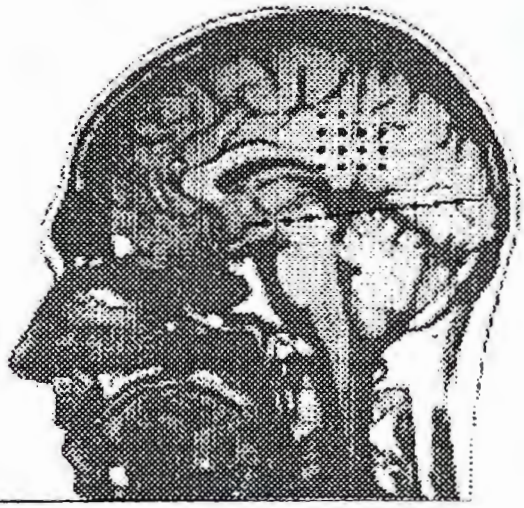

Proceedings

TU-BioMed Symposium 1998

"Brain Modelling"

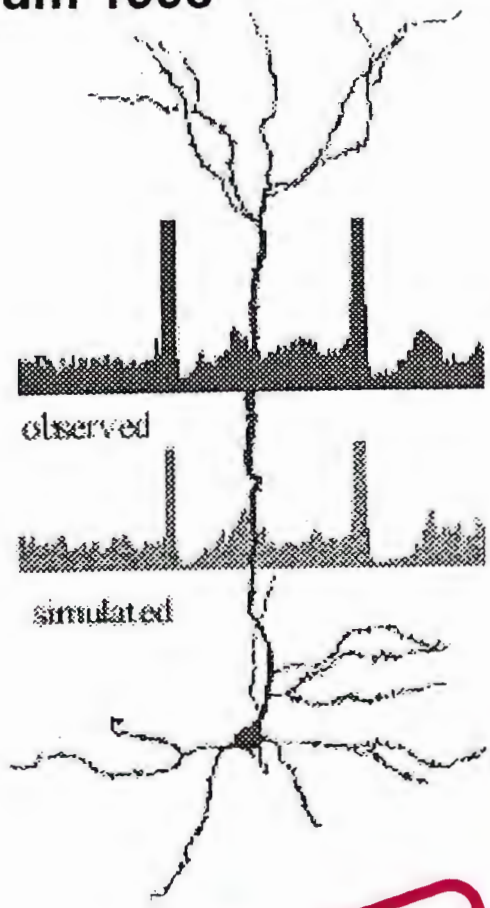

F. Rattay ed.

ISBN 3-901608-10-9

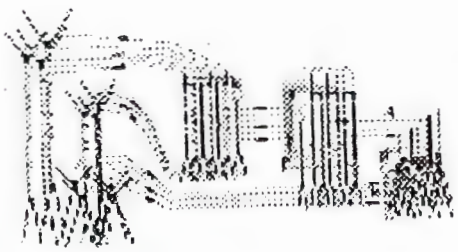

ARGESIM Report

ARGESIM Report

ARGESIM Report

ARGESIM Report No. 10
ISBN 3-901608-10-9

ARGESIM Reports
Series Editor: Prof. Dr. F. Breitenecker

ARGE Simulation News (ARGESIM)
c/o Vienna University of Technology
Wiedner Hauptstraße. 8-10, A-1040 Vienna, Austria
Tel: +43-1-58801-5386, -5374 Fax: +43-1-5874211
Email: info@argesim.org
WWW: http://www.argesim.org

TABLE OF CONTENTS

Brain Modelling - today

BRAIN MODELLING - today, this is a broad field between the disciplines. On one hand we are interested to explore the biophysical laws that describe the molecular events - and such questions go down to the level of quantum physics, an example is given by GUSTAV BERNROIDER in his contribution on *Quantum neurodynamics and its relation to cognition and consciousness*. At the next level of scaling the gating mechanisms at the ionic channels are very important for information processing and data distribution. Noise influence will be of great importance in order to detect weak signals and sometimes stochastic resonance is believed to accomplish real wonder - beyond the laws of physics, compare DONATELLA PETRACCHI - *Neural encoding: what stochastic resonance cannot do and what possibly it could do*, or ILLE GEBESHUBER and coworkers' *Stochastic resonance in the inner ear: the effects of endogenious transduction channel noise and stereociliary thermal motions on the human hearing threshold in various frequency bands* where it is demonstrated that nature tries to make profit from everything it can catch even when it is the thermal noise, which - up to now - was assumed to perform the border for sensory detection.

Nonlinear effects dominate the reactions at the level of the single neuron. Computational neuroscience is a new quickly expanding field that uses the powerful computers that are now available to simulate the reactions along the complicated shapes of neural elements. One technique is presented by FRANK RATTAY: *Simulation of neural excitation with compartment models*. This method is very useful to study the influences of membrane compositions on the reactions of a target neuron. We should be aware of the fact that changes of ion channels concerning types and densities are responsible for the individual behavior of functional neural subunits like initial segment, node and internode etc. Worldwide there are rather few investigations to simulate complete neurons or even soma-axon combinations. Examples are given by ALEXANDER STAENKE & Co *Spike Propagation in Aplysia Neurons* and by VINCENT STÜGER & Co *Modeling the electrical excitation of the mammalian auditory nerve*. Furthermore, the compartment model technique (which was already used by the early investigators like HODGKIN & HUXLEY in order to simulate neural signaling) can also be used in related fields - as demonstrated by MARTIN REICHEL & Co in the contribution *Computer simulation of denervated muscle by skin electrodes*. Another technical application that was developed by FRANK RATTAY from compartment modeling is to investigate *The contribution of a single neuron to the EEG signal and an attempt to explain the cochleogram*.

The EEG signal as it reflects the activities of a great number of neurons is rather difficult to interpret. MARIKE ESSL tries to analyze with mathematical tools simulated signals: *Simulation of EEG signals with autoregressive models* and OLIVER FILZ & Co investigate in Properties of Interhemispheric EEG Coherence during Sleep. HERBERT BAUER demonstrates that the EEG is able to show cognitive functions in his contribution on *Slow Potential Topography and Cognitive Anatomy.*

Furthermore, the nonlinear theory is applied to brain dynamics in CLAUDIA MONGINI & Co's contribution on *Non-linear dynamics and biological neuronal ensembles: application of Chaos Theory to analysis and modelling.*

But even the simplest neural nets as for example the touch reflex need a lot of nonlinear mathematics to be simulated. This is demonstrated by RICHARDSON NAVES LEAO and coworkers in *A Flexor and Crossed Extensor Reflexes Model using Neural Networks.* In this contributions artificial neural network techniques are shown to be nowadays a powerful tool in control technique. This means that - in spite of the fact that we currently are far away from a complete understanding of our brain - we use in technical applications methods that are copied from biology. However, the artificial neural nets still have essential shortcomings compared to the biological ones - that is demonstrated by ALICE MLADENKA & Co in *Biological and Artificial Neural Nets: A comparison.*

One fact that is not considered in artificial neural nets is the temporal component. Compartment models as introduced in the beginning are high above the molecular level. Nevertheless up to thousands of nonlinear differential equations that describe the membrane along a single neuron do not allow to simulate the temporal influence even in small nets of biological neurons. A new method to simulate biological neural nets is proposed by PETER SLOWIK & Co in *A novel neurosimulator to predict propagation of information in neuronal systems.* This program takes care on the traveling time of a neural impulse from his point of generation until to the synaptic contacts and with a rather simple method for calculating the traveling times it is possible to simulate the biological way of data processing in small neural nets about thousand times quicker compared to the compartment model approach.

Frank Rattay

Vienna, February 27, 1998

Simulation of Neural Excitation with Compartment Models

Frank Rattay
TU-BioMed Vienna University of Technology
Email: frattay@email.tuwien.ac.at

Introduction

A breakthrough in our understanding of the physics of neural signals which propagate as membrane voltage along the nerve fiber (axon) was achieved by the ingenious work of Hodgkin and Huxley (1952). To explore the complicated gating mechanism of the ion channels a long non-insulated wire was used as stimulating electrode, and thereby every part of the neural membrane had to react in the same way, i.e. propagation of signals was prevented. Refinements of their method as well as the application of patch clamp techniques (Neher and Sakmann, 1976) supply us with models for different neural cell membranes. With such models reliable prediction of membrane voltage V as a function of time is possible for arbitrary stimulating currents (comp. Rattay 1990,1993; Belluzzi and Sacchi 1991, DeSchutter and Bower 1994 or Staenke et al. this volume). The main equation has always the same form: One part of the stimulating current resulting from synaptic inputs or from an inserted electrode is used to load the capacity C of the cell membrane and the other part passes through the ion channels, i.e.

$$I_{stimulus} = C_m \frac{dV}{dt} + I_{ion}$$

and the velocity of voltage change becomes

$$\frac{dV}{dt} = \left[-I_{ion} + I_{stimulus}\right] / C_m \quad (1),$$

where the ion currents I_{ion} are calculated from appropriate membrane models. Usually, the membrane models are formulated for $1cm^2$ of cell membrane and the currents in eqn. (1) become current densities.

A positive stimulating current applied at the inside of an axon or at any other part of a neuron will cause an increase of V according to eqn. (1) if the membrane has been in the resting state before. In order to generate a spike this positive stimulus current has to be strong enough to reach threshold voltage. Threshold voltage causes many of the voltage sensitive sodium channels to open, and by sodium current influx (from the sodium rich extracellular fluid) the voltage increases to an action potential without the need of further stimulating support. A negative stimulating current applied at the inside will cause hyperpolarization (Fig. 1A, B).

Fig. 1. Computed reactions of a simple model neuron stimulated from the inside (upper traces) and from the outside (lower traces). The neuron consists of different subunits (comp. Fig. 2). Stimulation with negative and positive 0.1ms current impulses at the inside of the cell body (A, B) and by an extracellular microelectrode 0.5mm away from the center of the cell body (C, D) as indicated by the tips of the arrows.
Every line shows the membrane voltage of a single compartment as function of time. A: local hyperpolarization, B: an action potential propagates towards the branching terminal region. Extracellular stimulation generates stimulated and hyperpolarized zones within the neuron in both cases C and D. Strongest reaction is within the axon, at a position which is rather far away from the electrode, especially in D.

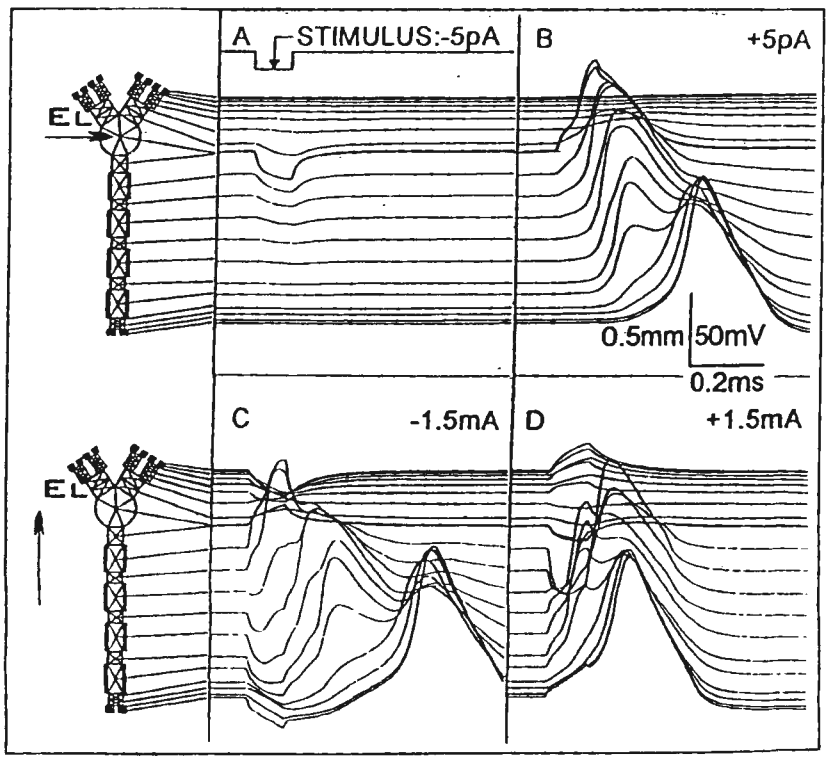

Compartment models

Current injection at the soma causes a situation rather similar to that of the 'space clamp' experiment of Hodgkin and Huxley: When the impulse is applied the strongest reaction is at the soma, but some of the injected current flows along the neuron and thereby the membrane voltages in the neighborhood of the soma is changed. (Fig.1 A, B).

Even a simple model of a neuron should consist of different subunits as shown in Fig. 2. A subunit is sometimes divided into several compartments small enough that the voltages at the inside ($V_{i,n}$) and at the outside ($V_{e,n}$) of the n-th compartment can be represented by a mean value. Every compartment has its individual shape and geometric and electric parameters.

According to Fig. 2 the current to the center point of the n-th compartment consists of a capacitive component, ion currents across the membrane and ohmic currents to the left and right neighbors, i.e. applying Kirchhoff's low results in

$$\frac{d(V_{i,n}-V_{e,n})}{dt}\cdot C_{m,n}+I_{ion,n}+\frac{V_{i,n}-V_{i,n-1}}{R_n/2+R_{n-1}/2}+ +\frac{V_{i,n}-V_{i,n+1}}{R_n/2+R_{n+1}/2}=I_{stimulus,n}$$

The stimulating influence to the neuron may be a synaptic input at the n-th compartment, or a current injection corresponding to $I_{stimulus}$ (not shown in Fig. 2), but for most compartments $I_{stimulus}$=0. With $V=V_i-V_e-V_{rest}$ we obtain the following system of differential equations for calculating the time courses of the reduced membrane voltages V_n: as a reaction of the compartments to the stimulating influence of the extracellular potential V_e:

$$\frac{dV_n}{dt}=\left[-I_{ion,n}+I_{stimulus,n}+\frac{V_{n-1}-V_n}{R_{n-1}/2+R_n/2}+\frac{V_{n+1}-V_n}{R_{n+1}/2+R_n/2}+\ldots +\frac{V_{e,n-1}-V_{e,n}}{R_{n-1}/2+R_n/2}+\frac{V_{e,n+1}-V_{e,n}}{R_{n+1}/2+R_n/2}+\ldots\right]/C_{m,n} \quad (2)$$

The dots in eqn. (2) are written for terms similar to the last one that have to be added in cases with more than two neighbor elements, e.g. at the cell body (soma) or in other branching regions.

Comparing eqn. (2) with (1) it is seen that the task of the stimulating current in every compartment can be performed by three components now: 1) the currents along the inside of the neuron, which are responsible for propagation of neural signals in natural situation (where V_e = 0 is usually assumed), 2) the currents resulting from the extracellular potentials ($V_{e,n-1}$, $V_{e,n}$, $V_{e,n+1}$) and 3) by current injection via synapses or inserted electrodes. According to point 1) - 3) the same compartment model can be used for the following applications, i.e. to simulate

- natural excitation (case 3a)
- excitation by current injection (case 3b)
- propagation of neural signals (case 1)
- artificial excitation or blockade of neural activites by applying electrical fields to the neural tissues (case 2).

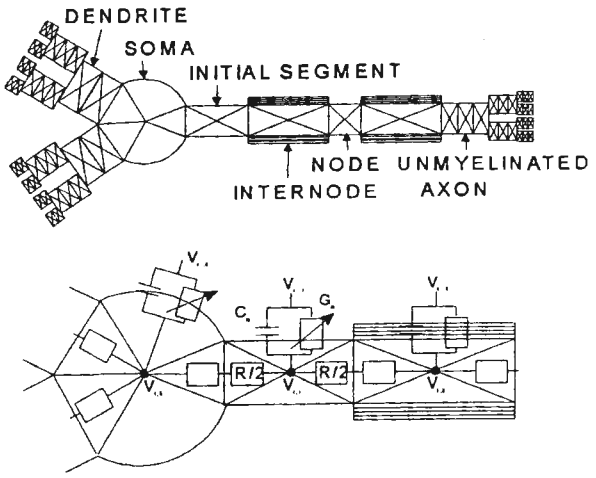

Fig. 2. Diagram of a neuron with subunits and part of an equivalent electrical network. Every subunit has its own membrane composition according to its physiological task. The electric parameters are shown for compartment 1: axoplasmic resistance to the neighbors (R/2 for cylinders), membrane capacity C_m and the membrane conductance G_m, which is only constant in compartments with passive membranes. In general, the ohmic membrane current consists of different types of ion currents that are governed by the rather complicated gating mechanisms of specific voltage sensitive ion channels.

Many published results on neural activities are based on compartment models, but most of them are concerned with axonal reactions only, where adequate membrane models are available. There exists rather few models for the different compositions of membranes of the other functional neural subunits.

Excitation by electrodes or by synaptic inputs - compartment models show the information processing along a neuron

Artificial excitation of a neuron can be done with extracellular electrodes. This technique is used in functional electrical nerve stimulation in order to allow deaf, blind and paralyzed patients to hear, to see and to move their limbs. With electric currents neural signals are also blocked in order to treat movement disorders or to suppress pain.

According to Eqn. 2 the influence of the extracellular potential on compartment n is

$$f_n = \left[\frac{V_{e,n-1}-V_{e,n}}{R_{n-1}/2+R_n/2}+\frac{V_{e,n+1}-V_{e,n}}{R_{n+1}/2+R_n/2}+\ldots\right]/C_{m,n} \quad (3),$$

which is the formulation of the "activating function" for neurons of arbitrary shape. The physical dimension of f_n is [Volt/sec] or [mV/ms], i.e. this form of the generalized activating function represents the velocity of voltage change in every compartment that is activated by the extracellular field. Changes in extracellular voltages, in the geometry and membrane capacity as well as the occurrence of branching elements cause irregularities in the sequence of f_n. In the case of a long straight unmyelinated axon the activating function becomes proportional to the second derivative of the extracellular potential along the axon (Rattay 1990).

The activating function is a powerful tool to obtain a first impression of the influence of an applied electric or magnetic field on a target neuron. Note that the information about stimulated (depolarized) regions, where f>0, and regions with hyperpolarizing effects (f<0) are obtained without any knowledge about the behavior of the voltage sensitive ion channels in the neural membranes.

In the following example the compartment model technique will be applied to the electrically stimulated human auditory nerve (details will be presented in a forthcoming paper).

The bipolar afferent mammalian auditory neuron connects the auditory receptor cell (inner hair cell) with neurons of the cochlear nucleus. In the natural situation a fluctuation (increase) of the receptor cell potential can cause a neurotransmitter release and thereby an action potential in the synaptic end of a fiber of the auditory nerve. This spike is generated in node0, passes the soma and travels along the central part of the axon. The geometry is shown in Fig. 3.

For simplicity we assume quasi-stationary potential distribution (neglecting tissue capacities) in an homogeneous extracellular medium. With this assumption the extracellular potential V_e can be calculated by

$$V_e = \frac{\rho_e I_{electrode}}{4\pi r} \quad (4)$$

where ρ_e is the extracellular resistivity and r the distance to the electrode, With Eqn. (3) the stimulating influence for every compartment can be calculated. The sign of the activating function f changes several times along the neuron (insert of Fig. 3) which means that the neuron consists of several activated and nonactivated (hyperpolarized) regions. Evaluation of the compartment model shows what is already predicted by the activating function: rather small changes in stimulus amplitude can change the points of artificial spike generation (Fig. 4). Fig. 5A shows the 'natural' spike generation by current entering the postsynaptic membrane of the first compartment which is simulated by current injection in node0.

node	Ve[mV]	f[V/s]
N0	445	607
N1	452	-3890
N2	339	2860
N3	300	61
N4	305	-421
N5	275	-2160
SOMA	175	9
N6	129	674

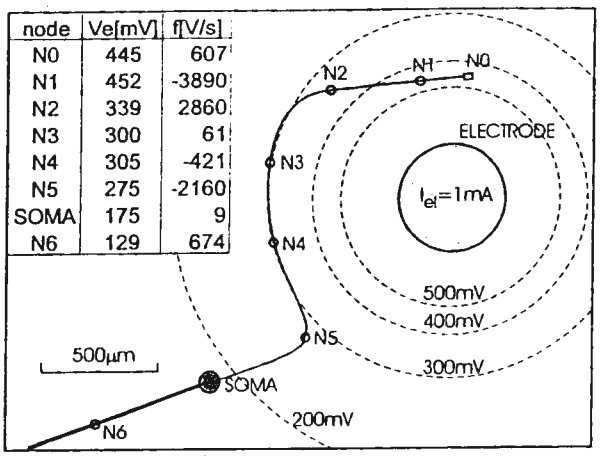

Fig. 3. Position of the human primary auditory nerve relative to a stimulating ring electrode which is inserted into a human cochlea. The mass electrode is assumed to be some mm away, the inhomogeneities in the conductive medium are neglected and therefore isopotential lines become circles. The inserted table shows the 'jumping' values of the activating function f when computed with one compartment per internode. Note the low value of f at node 3 caused by the nerve being close to an isopotential and that f_{soma} is still essentially lower, although V_e changes extensively. This low excitability is predicted by Eqn. 3 as a consequence of the high capacity of the soma membrane.

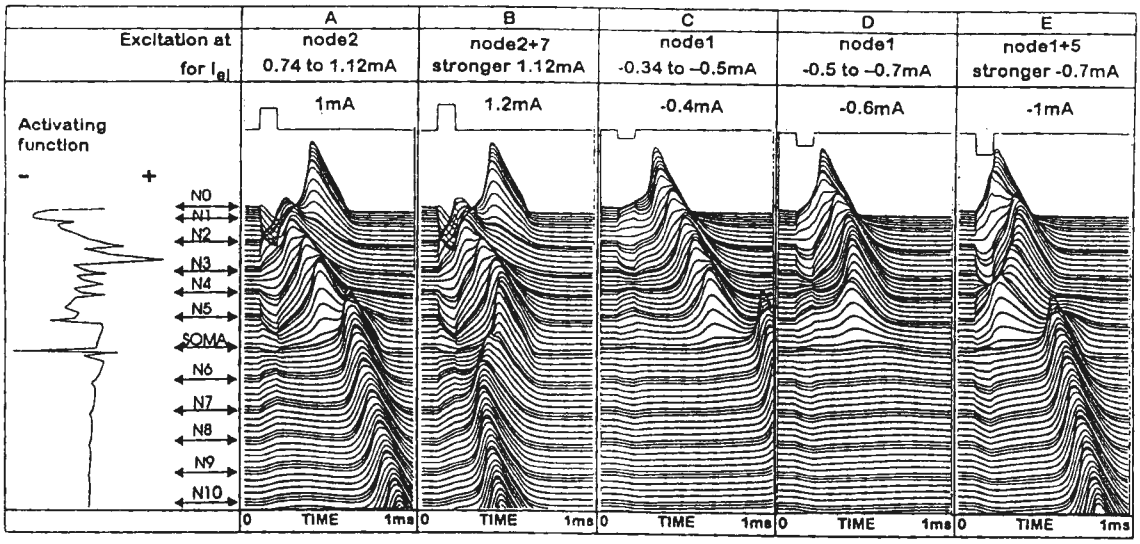

Fig. 4. Spike generation in a primary human auditory neuron by 100μs pulses. According to the activating function (left) the neuron is most excitable at node2 for positive stimuli; the maximum of f is within the passive membrane of the third internode. For negative electrode currents f predicts stimulating influence at node1, at node5 and at the unmyelinated part in front of the soma. Firing behavior changes when signal strength is varied. Every line in (A-E) shows membrane voltage for every compartment as function of time. Soma voltage appears as a single dark line in the center because of similar signal shape of soma and the two neighbored compartments with a center distance of 12.5μm to soma; reaction at nodes are center of triple lines. Note the delay in the axonal part when a 'dendritic' action potential passes the soma region (A,C,E). The rather small hyperpolarizing influence in the last dendritic internode hinders spike propagation into the axonal process (D).

Another application in functional electrical nerve stimulation is the blockade of neural activities by one side (antidromic) firing (Fig. 5C,D)

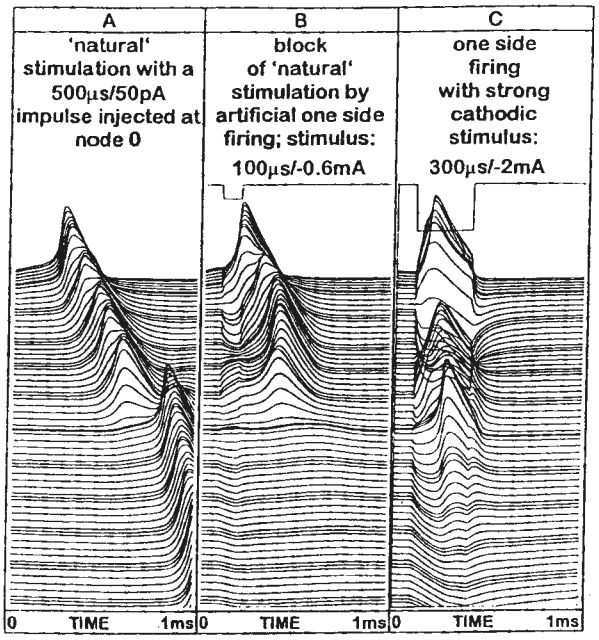

Fig. 5. Blockade of neural impulses by cathodic currents. (A) Simulation of synaptic excitation of neuron3. (B) Applying synaptic current and the block current as shown in Fig. 4D hinder excitation of the soma region. (C) A long strong cathodic pulse produces hyperpolarization of the axon, the soma becomes excited but not node6.

References

Belluzzi O. and O. Sacchi. 1991. A five conductance model of the action potential in the rat sympathetic neurone. Progr. Biophys. molec. Biol. **55**, 1-30

DeSchutter E. and J.M. Bower. 1994. An active membrane model of the cerebellar Purkinje cell: I. Simulation of current clamps in slice. J. Neurophysiol. **71**, 375-400

Hodgkin A.L. and A.F. Huxley. 1952. A quantitative description of membrane current and its application to conduction and excitation in nerve. J. Physiol. **117**, 500-544

Neher E. and B. Sakmann. 1976. Single-channel currents recorded from denervated frog muscle fibres. Nature **269**, 799-802

Rattay F. 1990. *Electrical Nerve Stimulation: Theory, Experiments and Applications.* Springer. Wien - New York

Rattay F. 1993. Simulation of artificial neural reactions produced with electric fields. Simulation Practice and Theory **1**,137-152

Staenke A., F. Rattay, H. Markum, M. Zartl and J. Hoyer 1998. Spike Propagation in Aplysia Neurons (this volume)

The contribution of a single neuron to the EEG signal - and an attempt to explain the cochleogram

Frank Rattay
TU-BioMed Vienna University of Technology
Email: frattay@email.tuwien.ac.at

Introduction

Although the electroencephalogram (EEG) was discovered more than a century ago and in spite of the fact that it is an important diagnostic tool, much remains to be clarified about the nature and the origin of the EEG. In order to understand the EEG signal as a result of collective effects within a neural network it seems important to investigate the contributions of the subunits of a single active neuron.

This article presents a method for estimating the potential distribution around a neuron, generated by its membrane currents. A two step routine is proposed to study the contribution of a single neuron to the EEG under quasi-stationary assumptions: At first the target neuron is represented by a chain of compartments, and in every compartment the total current across the neural membrane is calculated as a function of time. In the second step these currents are assumed to be sinks or sources at the center points of the corresponding compartments and the resulting potential distribution around the active neuron is calculated by superposition.

Current influx and outflux along a neuron

The membrane voltages changes essentially along an active neuron: region 1 may be excited while region 2 is at this moment not influenced by the propagating action potential and it is in the resting state. Therefore every compartment has a size that is small enough to be represented by a single electric circuit*).

The currents across the neural membrane have an essential influence on the electric field in the surrounding of the neuron. High current densities occur at the nodes of Ranvier, they are smaller in unmyelinated axons or at the soma membrane, rather negligible are the currents across the internodes. The current flow at the n-th compartment of the neuron can be calculated from*)

$$\frac{dV_n}{dt}=\left[-I_{ion,n}+I_{stimulus,n}+\frac{V_{n-1}-V_n}{R_{n-1}/2+R_n/2}+\frac{V_{n+1}-V_n}{R_{n+1}/2+R_n/2}+\ldots+\frac{V_{e,n-1}-V_{e,n}}{R_{n-1}/2+R_n/2}+\frac{V_{e,n+1}-V_{e,n}}{R_{n+1}/2+R_n/2}+\ldots\right]/C_{m,n} \quad (1)$$

where V_n denotes membrane voltage, $R/2$ is the resistance from the center to the border of the n-th compartment and $C_{m,n}$ is the membrane capacity (comp. Fig. 2 of Rattay 1998). Note that ion channel compositions changes essentially between neural subunits and it is of high importance to use in every compartment an adequate membrane model.

In the following example an action potential of a mammalian axon is travelling from the myelinated part into a non-myelinated (distal) region. The simulated axon consists of 12 nodes of Ranvier compartments calculated according to the CRSS model (Table 1) and 18 nonmyelinated segments with the same 6µm diameter (a 'warmed' HH model, with $k=12$ and doubled channel density, i.e. g_{Na}, g_K and g_L of the values in Table 1 are doubled). In the first segment a 0.1ms injected current impulse generates a propagating spike that is - with some difficulties - able to propagate into the unmyelinated terminal (Fig. 1).

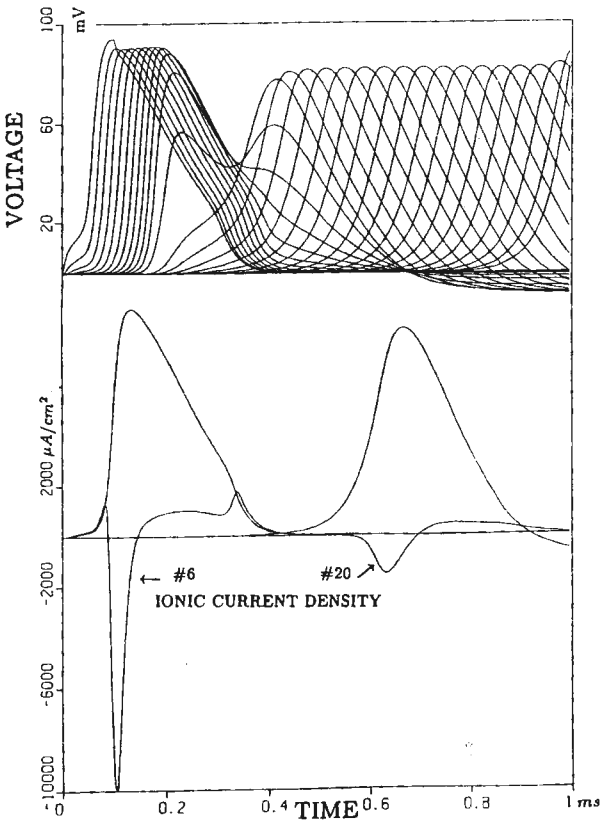

Fig. 1. Membrane voltages in a 30 compartment axon (top). The bottom traces show a copy of the action potentials of compartment #6 (node) and at #20 (unmyelianted axon) as well as the ion current densities. After 0.45ms membrane voltage and current are close to the resting values whereas compartment 20 starts to react at this time.

*) An introduction to the compartment model technique is found in the companion paper of this volume (Rattay 1998).

Note that the current densities at the nodes are about 10 times higher compared to that of the unmyelinated terminal (Fig. 1, bottom); but the current per unit length of the terminal is essentially higher because the nodal membrane segments are very short compared to the internodes (comp. e.g. Rattay 1995).

Significant contributions of current flow can be expected by collective effects in axons with a high degree of branching when a single neural impulse from the initial segment generates up to thousands of action potentials which arrive within a short time at the synaptic endings of the axonal tree. This effect is demonstrated in principle by the next 108 compartment model neuron which consists of a single dendrite (10 compartments), soma, initial segment, myelinated axon with 6 nodes and 7 internodes. The neuron is stimulated by a 0.05mA/10µs current pulse injected at the soma. On its way to one of the 16 end-compartments of the terminal region the generated action potential passes 30 compartments and four points of bifurcation. Propagation is delayed at the transition from the myelinated to the unmyelinated part of the axon (the same effect is seen in Fig. 1) and at every bifurcation (Fig. 2).

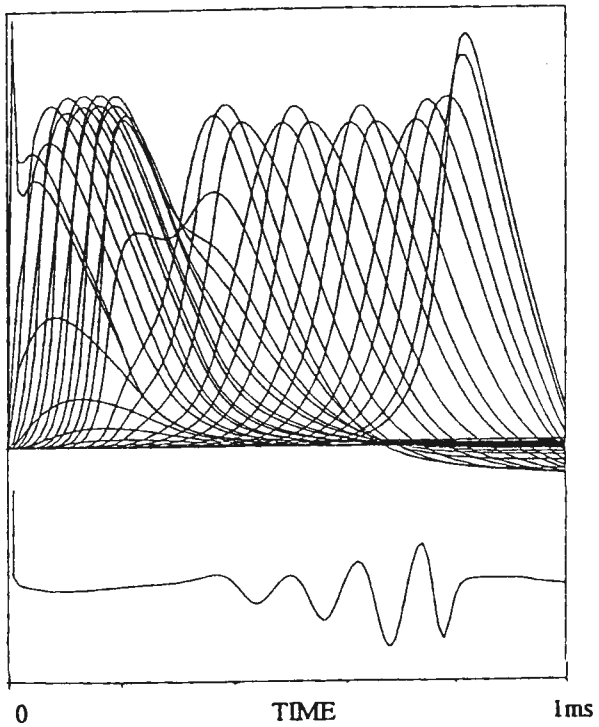

Fig. 2. Membrane voltages as functions of time. Because of symmetry in the branches there are only 40 different curves. The two high spikes (in the soma and in the initial segment) at the beginning result from the injected current, leading to a propagating action potential in the axon and an increase of voltage in the dendrite. The changes in propagation velocity are caused by the bifurcations of the axon and lead to oscillations in the extracellular potential.
The lower curve shows the extracellular potential calculated at 1mm above the soma.

Now we assume an infinite homogeneous extracellular medium with a current I from a single point source. The potential V_e at a distance r becomes

$$V_e = \frac{\rho_e I}{4\pi r} \quad (2)$$

where ρ_e is the extracellular resistivity. With Eqn. 1 we calculate in a first step the time evolution of the membrane currents for every compartment

$$I_n = I_{ion,n} + C_{m,n} \cdot \frac{dV_n}{dt} \quad (3)$$

The membrane currents are shown along the neuron in Fig. 3. After calculating these membrane currents every center point of a compartment is considered as a current source and the sum of their contributions describes the influence of the single neuron activity at a point of interest:

$$V_e(t) = \sum_n \frac{\rho_e I_n(t)}{4\pi r_n} \quad (4)$$

The resulting EEG contribution of the 108 compartment model neuron for an electrode positioned 1 mm above the soma is shown at the bottom of Fig. 2. An analysis of the computer simulation of this simple model neuron demonstrates that

1. the EEG contribution from the myelinated axon is rather small, compared to that of the soma,
2. the branching parts of the terminal can cause velocity reduction
3. the influence of some positive membrane currents can be annulled by negative currents from other regions of the same neuron.
4. collective effects (in the branching terminal) can be essentially stronger than from compartments close to the electrode.

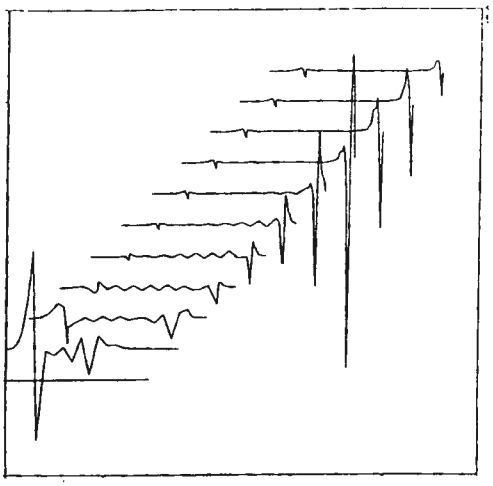

Fig. 3. Snapshots of membrane currents along a neuron in ten time steps. Note the strong signal at the beginning (line2, t=0.1ms) caused by the soma and initial segment and the even stronger currents at the terminal end (line 8, t=0.7ms) caused by the neural impulses when they reach the 16 terminal segments. The zigzag in lines 2-7 results from the different behavior of node and internode in the myelinated axon.

The cochleogram

The electrically evoked activities in the human auditory nerve can be measured with some of the electrodes of a modern cochlea implant. In the same way as for stimulation the measurement electrodes are positioned rather close to the neurons The neurons of the auditory nerve are bipolar and both processes are myelinated (comp. Fig. 3 of Rattay 1998 for the shape of the nerve relative to the electrode).

When stimulated naturally there is a time delay of about 300µs when the action potential crosses the soma region. This effect is similar to that observed in Fig. 1 when the low energy consuming myelinated fiber has to drive the spike into the energy vasting unmyelinated part (delay of spike). In case of human auditory nerves the energy of the spike of the periphery axon has to increase the membrane voltage of the relative large soma region which again causes a delay (comp. Fig. 5A of Rattay 1998 and Stüger et al. 1998). Such disturbances in propagation will also occur when the neurons are stimulated electrically (comp. Fig. 4 of Rattay 1998 and Stüger et al. 1998) and this may be the reason for the double peak in the cochleogram (Fig. 4). However such double peaks occur only in part of the measurements, an effect that may be related with the point of stimulus generation and perhaps in a greater number of degenered peripheral axons in patients that show no double peak responses.

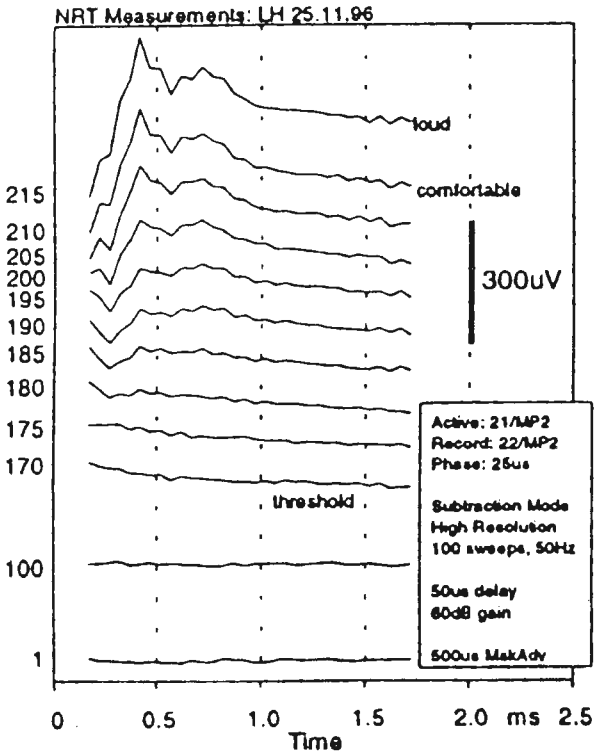

Fig. 4. Neural response telemetry from an human cochlear nerve that is electrically stimulated with increasing intensities. Note the double peaked signal. Reproduced from Dillier et al. 1997.

With the technique as described above we have calculated the voltage fluctuations resulting from the spiking of a single neuron under the simplified assumption of an infinite homogeneous extracellular medium (Fig. 5).

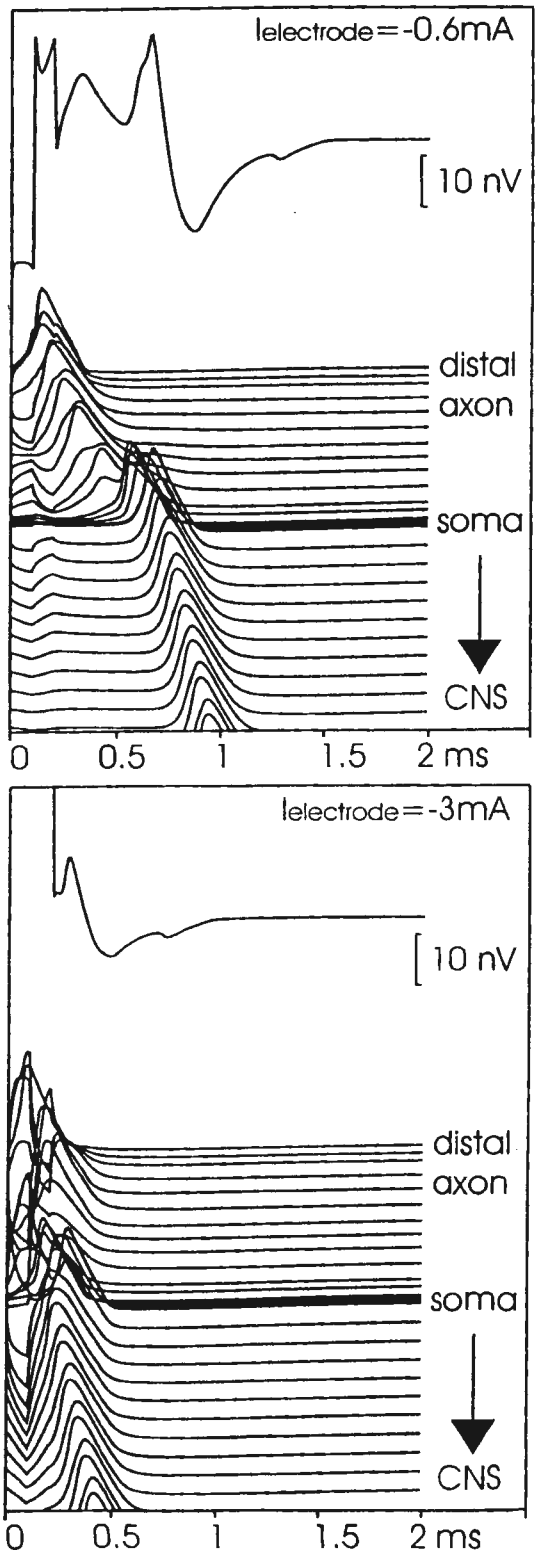

Fig. 5 Simulated nerve reactions for weak and strong biphasic stimuli. Upper traces: extracellular voltages at the electrode, lower traces membrane voltages along the neuron as functions of time. Note the double peak in one case only.

References

N. Dillier, W.K. Lai, M. Wyttenbach, H. Jakits, T. Spillman, T. Linder and U. Frisch 1997. First experiences with neural response telemetry (NRT) Report ENT Department University Hospital Zürich

F. Rattay 1990. Electrical Nerve Stimulation. Springer. Wien - New York

F. Rattay 1995. Propagation and distribution of neural signals: a modeling study of axonal transport. Physics of the Alive. 3, 60-67

F. Rattay 1998. Simulation of neural excitation with compartment models (this volume)

V. Stüger, F. Rattay and P. Lutter 1998. Modeling the electrical excitation of the mammalian auditory nerve (this volume)

HODGKIN-HUXLEY MODEL

$$\dot{V} = [-g_{Na}m^3h(V - V_{Na}) - g_K n^4(V - V_K) - g_L(V - V_L) + i_{st}]/c \quad \text{(HH-1)}$$

$$\dot{m} = [-(\alpha_m + \beta_m) \cdot m + \alpha_m] \cdot k \quad \text{(HH-2)}$$

$$\dot{n} = [-(\alpha_n + \beta_n) \cdot n + \alpha_n] \cdot k \quad \text{(HH-3)}$$

$$\dot{h} = [-(\alpha_h + \beta_h) \cdot h + \alpha_h] \cdot k \quad \text{(HH-4)}$$

with the coefficient k for temperature T (in ^oC)

$$k = 3^{0.1T-0.63} \quad \text{(HH-5)}$$

and

$$\alpha_m = (2.5 - 0.1V)/(exp(2.5 - 0.1V) - 1)$$

$$\beta_m = 4 \cdot exp(-V/18)$$

$$\alpha_n = (1 - 0.1V)/(10.(exp(1 - 0.1V) - 1)$$

$$\beta_n = 0.125 \cdot exp(-V/80)$$

$$\alpha_h = 0.07 \cdot exp(-V/20)$$

$$\beta_h = 1/(exp(3 - 0.1V) + 1)$$

$$V_{rest} = -70[mV]$$

$$V_{Na} = 115[mV], V_K = -12[mV], V_L = 10.6[mV]$$

$$g_{Na} = 120[k\Omega^{-1}cm^{-2}], g_K = 36[k\Omega^{-1}cm^{-2}]$$

$$g_L = 0.3[k\Omega^{-1}cm^{-2}], c = 1[\mu F/cm^2]$$

$$m(0) = 0.05, n(0) = 0.32, h(0) = 0.6$$

CRRSS MODEL

SWEENEY *et al.* (1987) transformed the original data of CHIU, RITCHIE, ROGERT & STAGG (1979) from experimental temperature $T = 14^oC$ to $T = 37^oC$. The following equations are called after the investigators the CRRSS model.

$$\dot{V} = [-g_{Na}m^2h(V - V_{Na}) - g_L(V - V_L) + i_{st}]/c \quad \text{(CRRSS-1)}$$

$$\dot{m} = -(\alpha_m + \beta_m) \cdot m + \alpha_m \quad \text{(CRRSS-2)}$$

$$\dot{h} = -(\alpha_h + \beta_h) \cdot h + \alpha_h \quad \text{(CRRSS-3)}$$

with

$$\alpha_m = (97 + 0.363V)/(exp((31 - V)/5.3) + 1)$$

$$\beta_m = \alpha_m/(exp((V - 23.8)/4.17))$$

$$\alpha_h = \beta_h/(exp((V - 5.5)/5))$$

$$\beta_h = 15.6/(1 + exp((24 - V)/10))$$

$$V_{rest} = -80[mV]$$

$$V_{Na} = 115[mV], V_L = 0.01[mV]$$

$$g_{Na} = 1445[k\Omega^{-1}cm^{-2}], g_L = 128[k\Omega^{-1}cm^{-2}]$$

$$c = 2.5[\mu F/cm^2]$$

$$m(0) = 0.003, h(0) = 0.75$$

Table 1. *Comparison of equations for membrane dynamics of unmyelinated and myelinated axons. V denotes the reduced membrane voltage in mV ($V = V_{membrane} - V_{rest}$); V_{Na}, V_K, V_L voltages across the membrane, caused by different (sodium, potassium, unspecific) ionic concentrations inside and outside the axon; g_{Na}, g_K, g_L maximum conductance of sodium, potassium and leakage per cm^2 of membrane; m, n, h probabilities for ionic membrane gating processes; α, β opening and closing rates for ion channels; c the capacity of membrane per cm^2; $m(0)$, $n(0)$, $h(0)$ values at the resting condtion where $V(0)=0$; i_{st} stimulus current.*
Note the high conductances and the missed potassium currents in the myelinated mammalian node as described by the CRRSS model.

Properties of Interhemispheric EEG Coherence during Sleep

O. Filz[1], P. Rappelsberger[2], J. Zeitlhofer[3], P. Anderer[4]

[1] Institute of Information Processing, Austrian Academy of Sciences
[2] Institute of Neurophysiology, University of Vienna
[3] Department of Neurology, University Hospital of Vienna
[4] Department of Psychiatry, University Hospital of Vienna

Summary

In this study, coherence analysis was applied to all-night EEG sleep recordings of 10 healthy volunteers in order to find criteria for an automatic classification of sleep stages. Spectral estimates were computed for 30 sec sleep stages obtained by visual scoring. Interhemispheric coherence between parasagittal leads (F3-F4, C3-C4, P3-P4, O1-O2) showed high dependence on sleep stages. The comparison of stages S1-W and REM-W showed similar results: in frequency bands Delta2 and Theta1 higher coherence was found during REM and during S1 compared with W in frontal, central and parietal regions. In Alpha and Sigma bands coherence was higher during W, most pronounced frontally and occipitally. S1-REM comparison showed higher coherence during REM, most dominantly in the central region. S2-S1 comparison revealed higher coherence during S2 in Delta1 with decreasing difference from frontal to occipital. In Alpha and Sigma bands coherence was higher during S1 frontally but it was higher during S2 parietally and occipitally.

Key words: sleep EEG, coherence, sleep stages

Introduction

This study deals with the contribution of coherence parameters for distinguishing sleep stages defined by the Rechtschaffen and Kales criteria (1968). Coherence is a spectral parameter that measures the correlation of frequency components of EEG signals derived from different locations on the scalp and may be interpreted as a measure for functional coupling or synchronisation of brain areas.

The criteria by Rechtschaffen and Kales were established to describe the sleep architecture of healthy subjects by visual inspection of 20 or 30 sec epochs. They define 7 discrete stages: Wake, REM, sleep stages 1, 2, 3, 4 and movement time. Rechtschaffen and Kales didn't introduce any topographic information of the EEG. The minimal configuration of a polygraphic recording is one EEG channel (either C3 or C4 referenced to the contralateral ear-lobe), two channels for vertical and horizontal eye movements and one channel for mental or submental EMG.

Nowadays we find a large number of studies dealing with multi-channel sleep EEG. For going beyond Rechtschaffen & Kales criteria, the examination of the micro-structure of sleep is of most interest. There are numerous results about spatial and temporal distribution of EEG parameters during sleep but only a few studies examin the cooperation of cortical areas using coherence or correlation analyses (e.g. Dumermuth et al. 1983; Nielsen et al. 1993; Corsi-Cabrera et al., 1996). Many of them can be hardly compared due to different recording and evaluation criteria but still they demonstrate that different brain states during sleep differ in EEG spectral parameters if coherence is considered. Therefor automatic sleep staging based exclusively on EEG spectral parameters appears promising. The visual scoring of polygraphic sleep recordings inheres the problem of subjective interpretation of rules. Coherence estimates may improve automatic classification and thus lead to a more objective assessment of sleep stages. At the same time they may provide additional information about the functional state of the brain.

Material and Methods

The study is based on whole-night sleep recordings of 10 healthy volunteers (7 females, 3 males, aged 20 to 35 years). EEG was recorded with 18 EEG electrodes according to the international 10/20 system, Fp2 was omitted, referenced to the average of both mastoid electrode signals. Band-pass settings were 0.5 to 30 Hz. EEG, 2 EOG channels and submental EMG were continuously written on paper. The whole-night sleep recording was divided into 10 minute periods: 7 minutes EEG and EOG were digitised continuously (sampling rate 102.4/s) and 3 minutes were needed for data storage on optical disc. The paper-records were visually scored according to Rechtschaffen and Kales (1968) criteria by 2 experienced electroencephalo-graphers. Time window was 30 sec.

Power spectra and cross-power spectra for the interhemispheric pairs F3-F4, C3-C4, P3-P4 and O1-O2 were computed using FFT and non-overlapping 2.5 sec epochs (256 samples) thus obtaining a frequency resolution of 0.4 Hz. Averaging in the time and the frequency domain yielded spectral parameters for the 30 sec epochs of the visual scoring in the frequency bands: Delta1 (0.4-2.0 Hz), Delta2 (2.4-3.6 Hz), Delta (0.4-3.6 Hz), Theta1 (4.0-5.6 Hz), Theta2 (6.0-7.6 Hz), Theta (4.0-7.6 Hz), Alpha (8.0-12.8 Hz) and Sigma (11.6-15.2 Hz). The final step was computation of coherence, the normalised cross-power spectrum.

Distribution of coherence was presented graphically for each sleep stage and each frequency band. In order to get quantitative measures of the distributions mean, median and lower and upper quartiles were estimated.

For a pairwise comparison of sleep stages, differences between the means and between the medians of corresponding frequency distributions were computed. In group studies this has the advantage that the results are independent of absolute coherence values which may vary considerably between subjects.

Only those results were considered significant when in at least 9 of the 10 subjects the same trend was observed, i.e. increase or decrease of coherence between stages. This corresponds to an error probability of $2\alpha \leq 0.05$ (sign test). The increase or decrease was considered weakly significant when it appeared in 8 of the ten subjects which corresponds to $2\alpha \leq 0.10$.

Results

The comparison of stage 1 (**S1**) and wake (**W**) shows significantly higher coherence during S1 frontally and centrally in the Delta2 band. There is also a trend of higher coherence during S1 in the Theta1 band frontally, centrally and parietally. In contrast, significant lower coherence occurred during S1 than during wake in the Alpha band frontally. Weakly significant lower coherence was also observed frontally and centrally in the Sigma band and occipitally in the Alpha-and Sigma band.

Coherence differences between **S2** and **S1** demonstrate a clear trend to higher coherence during S2. The only exception is S1 coherence in F3-F4 which is increasingly higher from the Theta1 to Sigma band. In the Delta1 band the difference between S2 and S1 is as high as 0.22 frontally and 0.15 centrally. Clearly higher coherence is also observed in the Sigma band parietally and occipitally. These results demonstrate that for differentiating sleep stages S2 and S1 interhemispheric coherences of Delta1 and Sigma bands seem to be most important.

Comparing stages **S3/4** and **S2** rather low differences not exceeding 0.05 were found. Most significant differences occurred in the Delta2, Theta1 and Theta2 bands frontally and the Delta1, Delta2 and Theta1 bands centrally, with higher S2 coherence. Contrary, weakly higher Alpha coherence during S3/4 was observed centrally and parietally. Summarising, the most significant differences between interhemispheric coherence during S3/4 and S2 were found in the frontal and the central regions, almost no differences appeared parietally and occipitally.

S1-REM comparison shows generally higher coherence during REM. Frequency bands mainly concerned are Delta2 to Alpha centrally with Theta2 and Alpha more pronounced and Delta2 parietally and occipitally.

The comparison between **REM** and **W** shows higher coherence during REM in the lower frequency bands Delta1 to Theta2, whereas coherence during wake was higher in the upper frequency bands Alpha and Sigma. Concerning location, the most essential results relate to frequency bands Delta2 and Theta1 from frontal to parietal and Alpha and Sigma frontally and occipitally.

Table I summarises the results of group analysis. We want to emphasize the differences between W, S1 and REM since these stages are usually difficult to distinguish.

Discussion

Scalp recorded EEG coherence turned out to be an essential large scale measure of functional relationships between pairs of neocortical regions. These measures are often closely related to cognitive or behavioural processes (e.g. Weiss and Rappelsberger, 1996; Rescher and Rappelsberger, 1996), but also to states of vigilance and sleep (e.g. Guevara et al., 1995).
Mathematically, coherence is defined as the squared normalised cross-power spectrum and may be interpre-ted as correlation coefficient in the frequency domain, i.e. correlation coefficient per frequency or frequency band. Coherence values can run from 0 to 1. Coherence 1 means that the corresponding frequency compo-nents of two EEG signals are identical and only amplitude differences and a constant time relation (phase delay) may exist. In case of coherence 0 the corresponding frequency components of both signals are not correlated.
The examination of the results of all ten subjects of the study showed considerable consistence concerning the global trends and correlation but also considerable differences concerning the absolute height of coherence values.
The problem inherent in almost all sleep analyses is the under-representation of some stages in the data, usually W and S1. This means that the results obtained for those stages are less reliable since they are based on a much lower number of epochs than e.g. the results for stages S2, S3/4 and REM. Nevertheless, the findings of group analysis are distinct and plausible.
In the EEG, stage S1 compared with W is characterised by an increase of the appearance of slow waves and a decrease of Alpha activity. In the interhemispheric coherence results this seems to be reflected by an increase in Delta2 and Theta1, however, predominantly only frontally and centrally. In the Alpha band coherence decreased most pronounced frontally and to a lesser degree occipitally. Coherence decrease in the Sigma band is closely related to the results in the Alpha band. This may be caused by our band definitions since there is a great overlap between both bands.
In stage S2 the characteristic EEG features are K-complexes and Sigma spindles. K-complexes have high portions of slow frequency components. This may result in the increase of Delta1 interhemispheric coherence when comparing S2 with S1. This increase is extremely pronounced frontally (0.22) and centrally (0.15). Regarding Sigma band and Alpha band the opposite interhemispheric coherence behaviour frontally on the one hand and centrally till occipitally on the other hand is striking. This may be caused by different properties of frontal and parietal frequency components represented by spindles (Trenker and Rappelsberger, 1996; Zeitlhofer et al. 1996; Broughton and Hasan, 1995). Coherence increase between both hemispheres (0.15 between P3-P4) may probably be due to highly coherent parieto-occipital spindle activities, i.e. closely linked cortical generators in both hemispheres. In contrast, frontal spindles seem to be generated by a different mechanism with dissociating frontal cortical areas caused by subcortical-cortical pathways leading to coherence decrease (-0.16 between F3-F4).
Only little coherence differences were found comparing S3/4 and S2. Most coherence decreases appeared frontally and centrally in the low frequency bands. This is rather surprising since enhanced slow wave activity during S3/4 was expected to lead also to higher coherence.
Coherence differences between stages REM and W were similar to those between S1 and W but more pronounced: higher coherence during REM in Delta2 and Theta1 frontally and centrally, lower coherence in Alpha and Sigma frontally and occipitally. The results give the impression that both Delta2 and Theta1 on the one hand and the very low Delta1 band on the other hand relate to different functional properties. Delta1 seems to be a good indicator for stage 2 and deeper stages whereas Delta2 and lower Theta seem to have selective power to distinguish between W and S1 and W and REM.
Distinction between S1 and REM by means of interhemispheric coherence turned out to be not very powerful. There is a trend of lower coherence centrally from Delta2 to Alpha but the differences do not exceed 0.07. For the determination of REM stage eye movements and muscle activity cannot be replaced.
Concerning frequency bands we found that for interhemispheric coherences there were almost no differences between Delta1 and the entire Delta band. On the other hand, high similarities between Delta2 and Theta1 coherences were found. In most of our comparisons of sleep stages those two bands showed about the same trends, except S1-REM comparison.
The presented study demonstrates relations between interhemispheric coherence and sleep stages which may support automatic sleep staging in combination with other parameters, like spindles, K-complexes, Delta power, rapid eye movements and slow eye movements.

		δ_1	δ_2	ϑ_1	ϑ_2	α	σ
S1-W	F3-F4		++	+		---	-
	C3-C4		+++	+			-
	P3-P4			+			
	O1-O2					-	-
S2-S1	F3-F4	+++		-	--	--	---
	C3-C4	+++					+
	P3-P4	++				++	++
	O1-O2	+	++		+		+++
S3/4-S2	F3-F4		--	---	--		
	C3-C4	--	--	--	-	+	
	P3-P4					+	+
	O1-O2	+					
S1-REM	F3-F4						
	C3-C4		-	-	---	--	
	P3-P4		--		-		
	O1-O2		--				
REM-W	F3-F4		++			--	--
	C3-C4		+++	++	+		
	P3-P4	+	+	++			
	O1-O2	+				--	--

Table I: Significant interhemispheric coherence differences between sleep stages as indicated in the left column. Positive difference: +++ (in 10 of 10 subjects); ++ (in 9 of 10); + (in 8 of 10); negative difference correspondingly.

Acknowledgement

This study was started in the framework of the BIOMED-1 concerted action ANNDEE (BMH1-CT94-1129) and it is continued within the BIOMED-2 project SIESTA (BMH4-CT97-2040), both sponsored by the European Commission, DG XII, and the Austrian Federal Ministry of Science and Research. For more information on SIESTA see: http://www.ai.univie.ac.at/oefai/nn/siesta/

References

Broughton R., Hasan J. (1995) Quantitative topographic electroencephalographic mapping during drowsiness and sleep onset. Journal of Clinical Neurophysiology 12(4): 372-386.

Corsi-Cabrera M, Guevara MA, Arce C, and Ramos J. (1996) Inter and intrahemispheric EEG correlation as a function of sleep cycles. Prog. Neuro-psychopharmacol. & Biol. Psychiat. Vol 20: 387-405.

Dumermuth G., Lange B., Lehmann D., Meier C.A., Dinkelmann R., Molinari L. (1983): Spectral analysis of all-night sleep EEG in healthy adults. Eur. Neurol. 22: 322-339.

Guevara MA, Lorenzo I, Arce C, Ramos J and Corsi-Cabrera M. (1995) Inter and Intrahemispheric EEG Correlation during Sleep and wakefulness. Sleep, 18: 257-265.

Nielsen, T., Montplaisir J., Lassonde M. (1993): Decreased Interhemispheric Coherence during Sleep in Agenesis of the Corpus Callosum. Eur. Neurol. 33: 173-176.

Rappelsberger P. and Petsche H. (1988): Probability Mapping: Power and Coherence analysis of cognitive processes, Brain Topography, 1, pp.46-54

Rechtschaffen A and Kales A, (Eds). (1968) A Manual of Stadardized Terminology, Techniques and Scoring System for Sleep Stages of Human Subjects. Los Angeles: Brain Information Service, Research Institute.

Rescher B. and Rappelsberger P. (1996): EEG-changes in Amplitude and coherence during a tactile task in females and in males, Journal of Psychophysiology, 10, pp.161-172

Trenker E., Rappelsberger P.: Requirements for automatic sleep spindle detection using artificial neural networks, Medical & Biological Engineering & Computing, 34, Part 2: 225-226, 1996

Weiss S. and Rappelsberger P. (1996): EEG coherence within the 13-18 Hz band as correlates of a distinct lexical organisation of concrete and abstract nouns in humans, Neuroscience Letters, 209, pp.17-20

Zeitlhofer J., Gruber G., Anderer P., Asenbaum S., Schimicek P., Saletu B. (1997): Topographic distribution of sleep spindles in young healthy subjects. J. Sleep Res. 6: 149-155.

Simulation of EEG signals with autoregressive models

M. Essl

Institute of Neurophysiology, Waehringerstrasse 17, A-1090 Vienna

Marike.Essl@univie.ac.at

1 Introduction

EEG coherence is an essential tool for the description of functional relationships between brain regions. This measure is defined as the squared normalised cross-power-spectrum of two signals (Jenkins and Watts, 1968).

However, EEG coherence is highly dependent on the recording technique, since the signal at the reference input of the differential amplifiers has a great influence on the shape of the EEG signals. In praxis, definite information about the properties of the reference signal is not available and can only be estimated based on pre-knowledge and experience. Unambiguous results can only be obtained by simulation studies using a data model with known spectral properties. A study concerning the reference problem when computing EEG coherence was presented by Essl and Rappelsberger (in press).

2 Method

EEG signals can be simulated according to assumed and pre-given properties. This can be realised by autoregressive processes (Rappelsberger, 1989). In the same way different reference signals can be simulated to study their influence on coherence.

2.1 Autoregressive models

Coherent EEG signals may be simulated by a two-dimensional autoregressive process of the first order:

(1)
$$x_t = a_{11} \cdot x_{t-1} + a_{12} \cdot y_{t-1} + z_{1t}$$
$$y_t = a_{21} \cdot x_{t-1} + a_{22} \cdot y_{t-1} + z_{2t} .$$

The signal x_t is dependent on its own past x_{t-1} and y_{t-1}, the past of the signal y_t. Signal y_t depends on its own past y_{t-1} and the past x_{t-1} of signal x_t. z_{1t} and z_{2t} are noise processes. The AR-coefficients a_{11}, a_{12}, a_{21}, a_{22} determine the spectral properties.

For the simulation of a reference signal which is incoherent to signals x_t and y_t, a one-dimensional AR-process of the third order can be used:

(2) $$r_t = a_1 \cdot r_{t-1} + a_2 \cdot r_{t-2} + a_3 \cdot r_{t-3} + z_{rt}.$$

The reference signal r_t is dependent on its own past r_{t-i} and the autoregressive parameters a_i for i=1,2,3, respectively. z_{rt} is a random process. This linear system (2) can be described as an linear filter with a random process z_{rt} at the input and the signal r_t at the output (Jenkins and Watts, 1968).

2.2 Stability criteria

Every linear system such as (1) and (2) can be characterised by its transfer function $H(f)$ in the frequency domain. Autoregressive processes can be seen as recursive linear filters. Since under certain circumstances these types of filters can start oscillating, stability criteria have to be considered. Therefore autoregressive-parameters must be selected with restrictions: The poles of the system need to lie inside the unit circle. Poles are given by the zeros of denominator of the transfer function.

2.3 Simulation

Modelling consists of: Spectral properties like e.g. a certain coherence value in a given frequency band are assumed. That means coherence between both signals x_t and y_t and spectral properties of the reference signal r_t are pre-given. The next step is computation of the corresponding autoregressive parameters using one- and two-dimensional processes. Then signals according to the computed autoregressive parameters are generated. EEG signals are simulated according to the differential amplifier condition. This is followed by the computation of coherence between the distorted signals. And finally, values of pre given coherence and coherence of simulated signals are compared and give a measure for the influence of the distortion, which depends on the properties of the reference signal.